2020 IEEE International Conference on Robotics and Automation (ICRA)
31 May - 31 August, 2020. Paris, France

# Design and Validation of a Soft Robotic Ankle-Foot Orthosis (SR-AFO) Exosuit for Inversion and Eversion Ankle Support

Carly M. Thalman, *Student Member, IEEE*, and Hyunglae Lee*, *Member, IEEE*

***Abstract*— This paper presents a soft robotic ankle-foot orthosis (SR-AFO) exosuit designed to provide support to the human ankle in the frontal plane without restricting natural motion in the sagittal plane. The SR-AFO exosuit incorporates inflatable fabric-based actuators with a hollow cylinder design which requires less volume than the commonly used solid cylinder design for the same deflection. The actuators were modeled and characterized using finite element analysis techniques and experimentally validated. The SR-AFO exosuit was evaluated on healthy participants in both a sitting position using a wearable ankle robot and a standing position using a dual-axis robotic platform to characterize the effect of the exosuit on the change of 2D ankle stiffness in the sagittal and frontal planes. For both sitting and standing test protocols, a trend of increasing ankle stiffness in the frontal plane was observed up to 50 $kPa$ while stiffness in the sagittal plane remained relatively constant over pressure levels. During quiet standing, the exosuit could effectively change eversion stiffness at the ankle joint from about 20 to 70 $Nm/rad$ at relatively low-pressure levels ($< 30$ $kPa$). Eversion stiffness was 84.9 $Nm/rad$ at 50 $kPa$, an increase of 387.5% from the original free foot stiffness.**

***Keywords*** - Soft Robotics, Wearable Robots, Assistive Robots, Rehabilitation.

## I. Introduction

Chronic ankle instability (CAI) is a long-term disability that is often the result of recurrent ankle sprains, where tendons surrounding the joint are extended past the natural length and permanent deformation occurs [1], [2]. Ankle sprains can occur when a sudden instance of inversion or eversion ensues due to unanticipated lateral ankle buckling, resulting in excessive stress to the tendons [2]. For reported ankle sprains, 85% of injuries can be attributed to lateral sprains [3]. Many reported cases of CAI continue to impact the affected individuals and can cause future risk of falls, trips, and injury from the ankle yielding as a result of loosened or damaged tendons [2], [4], [5]. These types of injuries usually occur in the frontal plane [2]. Current methods of CAI treatment commonly prescribe rigid ankle braces that serve as splints, using stiff plates placed along the medial and lateral malleolus of the ankle to prevent IE motions during walking and weight-bearing actions of the affected individual [4], [6]–[8]. Most ankle-foot orthoses (AFOs) are made from stiff, lightweight plastics that passively provide stiffness to the ankle joint to help increase balance and prevent lateral ankle buckling [4], [9], [10]. Rigid AFOs limit ankle motion and fix the joint at a neutral angle, which can subsequently lead to complications with mobility, increased risk of injuries, or pain due to gait adaptations attributable to limited ankle function [4], [5], [11], [12]. Wearable robotics designed to assist the ankle face several challenges including; weight, computationally heavy programming algorithms, joint alignment, and cost [9]. Soft robotic solutions have demonstrated successful designs for lightweight, cost-effective assistive devices with flexible materials and forgiving interactions between the robot and the intricate human ankle joint [13], [14]. The compliant materials used in soft robotics use less computing power for joint alignment, avoid heavy components on the foot, and provide comfortable actuation methods during ankle rehabilitation [15]–[18] and augmentation [9], [19]. While cable-driven systems have been used successfully in previous work [17], [19]–[21], there are limited studies for soft robotic applications that specifically address issues involved with CAI and lateral ankle sprain prevention that use a fabric-based approach or use pneumatic actuators to address the issue of providing variable stiffness.

This paper presents a soft robotic AFO (SR-AFO) exosuit (Fig. 1) to assist in inversion-eversion (IE) ankle support using pneumatic soft fabric actuators to increase IE ankle stiffness, with minimal impacts on ankle dorsiflexion-plantarflexion (DP) stiffness. The soft actuators are made


Fig. 1. Design of the SR-AFO exosuit incorporating the inflatable fabric-based actuators for inversion and eversion support. (a) A concept illustration of the SR-AFO exosuit being worn by a user, (b) A close up view of the SR-AFO exosuit being worn over the shoe, and (c) Internal layers and soft actuator placement.

* Corresponding Author
Carly M. Thalman and Hyunglae Lee are with the Ira A. Fulton Schools of Engineering, Arizona State University, AZ, USA. cmthalma@asu.edu, hyunglae.lee@asu.edu

from compliant fabric and pneumatically controlled to vary resulting actuator stiffness. The actively varying change in stiffness is used to prevent ankle buckling in the IE direction and provides a comfortable, dynamic solution that behaves as a garment when inactive and can be worn over the user's shoe. This paper also presents a novel approach to characterizing the resulting stiffness at the ankle for a soft AFO with variable stiffness focused on lateral support using pneumatic fabric-based actuators.

## II. Design of the SR-AFO Exosuit

### A. Design Criteria and Considerations for SR-AFO Exosuit

The SR-AFO exosuit was made from a custom neoprene fabric sleeve that wraps the leg shank and secures under the arch of the foot as shown in Fig. 1. The SR-AFO exosuit slips on easily like a boot, and the don/doff time was minimized by using adjustable Velcro straps that hold the SR-AFO exosuit with a snug fit around the ankle joint, yet still allows for comfortable and natural movement. The straps also provide additional anchoring points for the soft fabric actuators, ensuring minimal slippage once inflated. The soft fabric actuators were placed vertically on either side of the ankle, starting at the base of the talus and running across the medial and lateral malleolus of the ankle to mimic the placement of traditional ankle braces for medial and lateral instability, as shown in Fig. 2a. The SR-AFO exosuit was designed as a one-size-fits-all device and adapts to the foot size of most adult subjects. Inextensible nylon anchoring points were embedded in the lining of the neoprene sleeve brace to hold the actuators in place at the top and base of each actuator, as shown in Fig. 2b. This design allows the user to have freedom and comfort when wearing the device, but also to have controllable support in the IE direction with variable stiffness as needed.

A target threshold for IE stiffness was set for 70 $Nm/rad$. This value is significantly higher than the IE stiffness that unimpaired young individuals can achieve with the highest voluntary contraction of ankle muscles. Thus, the proposed design should be able to provide sufficient active support to the ankle in the frontal plane to reduce the risk of ankle sprains or injuries [22], [23].

### B. Fabrication and Control of Actuators

The SR-AFO exosuit pneumatic source was controlled using a portable air compressor (California Air Tools, Model 8010A, San Diego, CA), which was connected to a digital pressure sensor and pneumatic valve. This valve used manual inputs to change and increment pressure as needed for each individual, quasi-static test environments as described in future sections. The soft fabric actuators were made from a thermoplastic polyurethane (TPU) coated nylon fabric (200 Denier Rockywoods Fabrics). The coated nylon was oriented with the TPU coating facing inward and thermally bonded at predetermined geometries to allow for the desired actuator behavior and characteristics. The thermal bonds were created with a 2 *mm* heat impulse sealer (AIE-500 2 mm Impulse Sealer, American International Electric INC, CA) which

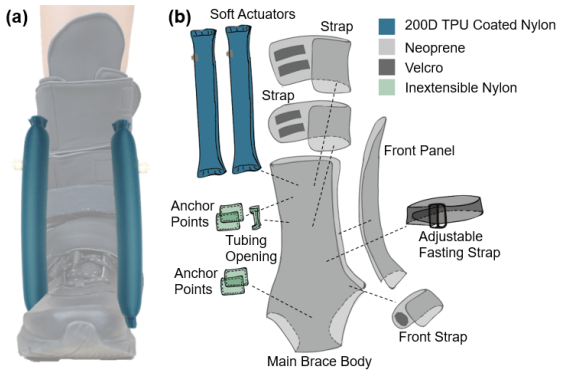


Fig. 2. (a) Frontal view of the SR-AFO exosuit showing the actuator placement along the ankle joint. (b) All of the layers and materials used in the fabrication of the SR-AFO exosuit in an exploded view, indicating layer placement.

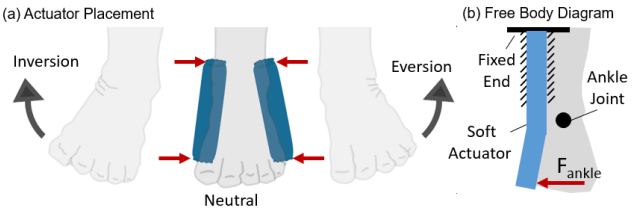


Fig. 3. Free body diagram of the soft fabric-based actuator in a cantilever orientation against the ankle. (a) a simplified illustration of the actuator placement and actuator interaction forces with the joint, and (b) the simulated orientation and boundary conditions set for modeling.

applied uniform heat and pressure to the seam to create an air-tight seal. This formed the geometrically programmed chambers for future inflation with the pneumatic control system. The actuators were fabricated using a single rectangular sealed pouch, which was then folded in half and sewn along the outside of the heat seal to form a loop. When inflated, this loop formed a hollow cylinder, which expanded inward to occupy the negative space inside the loop, similar to that of a blood pressure cuff.

## III. Characterization of the SR-AFO Exosuit

### A. Modeling of Fabric-Based Inflatable Actuators

Previous studies have shown successful applications of beam-like inflatable soft actuators, which consist of a single soft chamber inflated to form a rigid beam [16], [24], [25]. There have also been applications in which an inflatable actuator has been modeled as a hollow beam with negative space in the center [26], [27]. In the application of the SR-AFO exosuit, the presented actuator design minimizes actuator deflection to prevent ankle buckling in the IE direction without increasing internal volume. The design of the soft actuator was modeled using geometric programming of soft materials, where preliminary modeling was based on several initial assumptions that proved reliable in previous applications [28]. The assumptions used in this model: 1) when inflated, the fabric material was inextensible and maintained its net shape with minimal deformation to behave similarly to a rigid object; 2) the inflated shape assumed a simplified geometric shape when pressurized; 3)

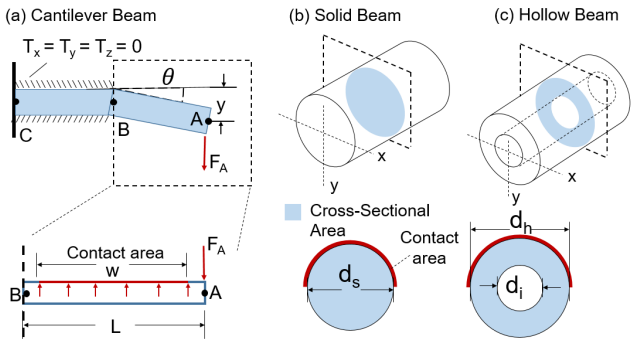


Fig. 4. (a) The assumed beam orientation used to model Castigliano's Theorem with a cantilever beam, applied moment, uniform workload and a dummy load, (b) the solid cross section of the first actuator design, and (c) the hollow cross section of second actuator design.

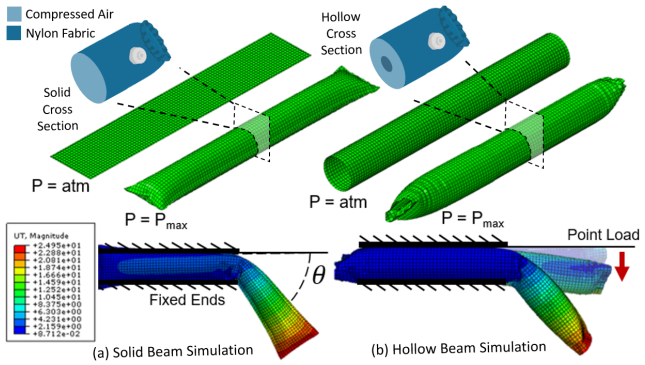


Fig. 5. FEA model of the soft actuators as extruded 2D shells, the depiction of the cross section at the center of each actuator and the model for the (a) solid and (b) hollow cross sections, after pressurization and loads have been applied to achieve deflection angle.

the internal pressure was uniform throughout the internal area. The payload capability of the actuator depends on various factors, including radius of the actuator, internal pressure, and direction of loading. Inspiration for the design of the soft inflatable actuators was drawn from Castigliano's Theorem used in beam theory for determining deflection of a cantilever beam [29], [30]. The soft actuators were modeled as a cantilever beam, fixed on all sides at one end and free to move at the other end - the end of the actuator running parallel to the ankle calcaneus (Fig. 3b). The actuator was modeled using a principle of beam theory to determine deflection of the cantilever beam, $y$:

$$y = \frac{1}{EI}\left(\frac{1}{3}F_A L^3 + \frac{1}{8}wL^4\right) \tag{1}$$

which was formulated using Castigliano's Theorem applied to a cantilever beam with a uniform workload ($w$) across the beam length ($L$) for internal pressure. A transverse load ($F_A$) (Fig. 4a) was applied at the free end of the beam. $E$ represents the elastic modulus, and $I$ represents the area moment of inertia for the cross-section of the soft actuator beam model (Fig. 4b-c). In this instance, $w$ was estimated using the following work to pressure relation,

$$w = \frac{PC_a}{L}, \text{ where } C_a = \frac{1}{2}Ld\pi \tag{2}$$

where the pressure ($P$) of the actuator acts across the contact area ($C_a$), resisting bending (top half of the circumference of the beam) and applied along length $L$. It was assumed that the volume of the internal chambers is equal to the total area of the beam, as indicated by the shaded regions in Fig. 4b-c. The workload resists bending and was found using the uniform internal actuator pressure across the area of contact. In this 2D representation, that area was the vertical edge of the beam over length $L$. The angle of deflection, $\theta$, was found for the beam using the following relation of the vertical deflection, $y$, and fraction of $L$ at which bending was allowed to occur.

$$\theta = sin^{-1}\frac{y}{L} \tag{3}$$

Using the theorem in Eq. (1), it was observed that the deflection decreases with a higher moment of inertia. To minimize the total actuator volume while increasing actuator moment of inertia, two actuator configurations were compared, modeled as rigid beams: (1) solid cylinder, and (2) thin-walled hollow cylinder. The area of the solid and hollow cross sections was held constant, and the relation was defined using the following conditions:

$$A_s = A_h \ , \ d_i < d_h, \text{ and } d_s = \sqrt{d_h^2 - d_i^2} \tag{4}$$

where the cross-sectional area ($A_s$) of the solid beam was set equal to the cross-sectional area of the hollow cylinder, $d_s$ was the diameter of the solid cylinder, and $d_h$ and $d_i$ were the outer and inner diameters of the hollow cylinder, respectively. This allowed for a higher moment of inertia, and therefore a higher resistance to beam deflection for the same volume. Using the parallel axis theorem and the conditions listed in Eq. (4), the second moment of inertia for the solid actuator designs was defined as:

$$I_s = \frac{\pi d_s^4}{64} = \frac{\pi(d_h^2 - d_i^2)^2}{64} \tag{5}$$

The second moment of inertia for the hollow actuator design was defined as:

$$I_h = \frac{\pi(d_h^4 - d_i^4)}{64} \tag{6}$$

Since $I_h > I_s$ for the same internal volume of a cylinder, less deflection was expected for the hollow cylinder design for $I_h$. This was validated in the following finite element analysis (FEA) and experimental studies.

### *B. Deflection vs Load Evaluation*

In order to evaluate the efficacy of the actuator design, a FEA study was used to model and simulate the soft fabric actuators using the materials properties found in previous work [15]. The FEA simulation was run using Abaqus CAE (ABAQUS, Dassault Systems, Vlizy-Villacoublay, France) in a dynamic explicit environment. Thin 2D homogeneous shells were used to create each layer of the fabric actuator, and sectioned partitions of the shells were tied to create seams. A uniform pressure force was applied across the innermost facing surfaces of the thin shells and increased in increments of 25 $kPa$ from 0 $kPa$ up to 100 $kPa$. The solid and hollow actuators were simulated using two separate

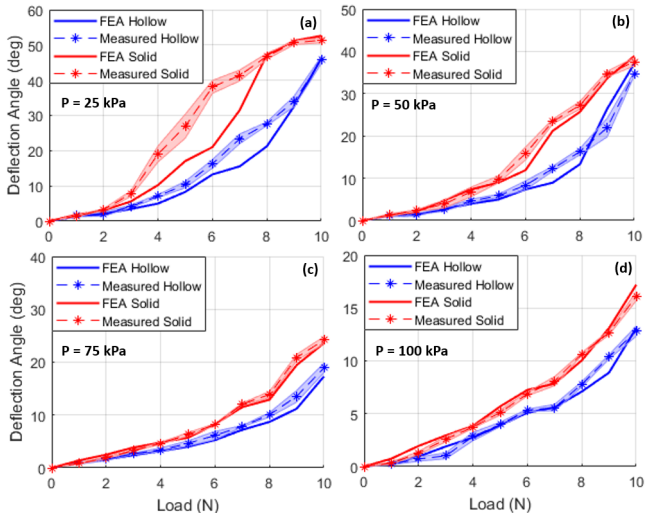


Fig. 6. Results of FEA analysis and experimentally measured values of the both the solid cross section actuator design and hollow cross section actuator design, and standard deviation represented by the shaded regions. (a) - (d) depicts the deflection angle for each actuator at 25 *kPa*, 50 *kPa*, 75 *kPa*, and 100 *kPa*, respectively.

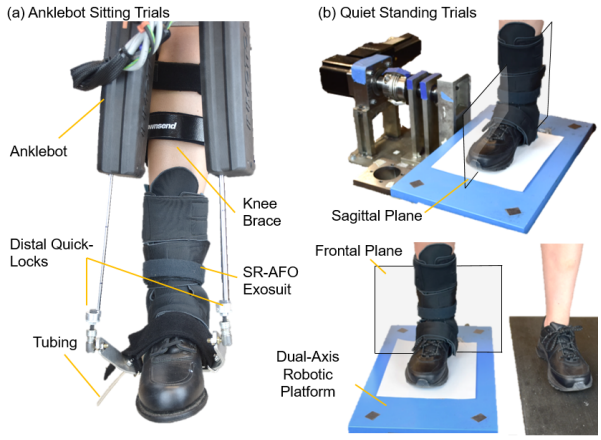


Fig. 7. (a) the Anklebot setup with the user wearing the SR-AFO exosuit over the custom Anklebot shoe, (b) the dual-axis robotic platform setup with the user wearing the SR-AFO exosuit for the measurement of IE stiffness in the frontal plane and DP stiffness in the sagittal plane.

models. This was done by using 1) two flat 2D surfaces tied at the edges to create a single chamber when a pressure load was applied (Fig. 5a), and 2) two overlapped extruded cylindrical shells tied at each end to seal a continuous volume chamber in the shape of a ring when the pressure load is applied (Fig. 5b). The beams were constrained by an infinitely stiff rigid component to execute a cantilever orientation as shown in Fig. 5. The following steps were completed at four pressure levels (25, 50, 75, and 100 *kPa*) for ten applied point loads (1-10 *N* in increments of 1 *N*): (1) Pressurization, (2) Stabilization, (3) Point Load. The deflection of the actuator was measured by fixing one half of the actuator along the y-axis, and applying a perpendicular force to the free end. Deflection was measured as the change in the angle from the starting position of the inflated actuator to the final position of the free end of the actuator as shown in Fig. 5.

The two actuator designs were evaluated experimentally. Actuator deflection was measured using quasi-static testing methodology in a cantilever orientation using a 3D printed housing. Actuator pressure was increased in increments of 25 *kPa* from 25 *kPa* to 100 *kPa*. For each pressure level, a vertical point load was applied to the end of the actuator from 1-10 *N* in increments of 1 *N*. For each pressure level and point load combination, the deflection of the actuator was measured using a goniometer for a total of three trials for each quasi-static condition. The actuators were less predictable at low pressures, shown by the middle of the curve in Fig. 6a. The maximum deflection angle for a 10 *N* point load at 25 *kPa* was $45.77 \pm 1.01^\circ$ and $51.32 \pm 0.71^\circ$ for the hollow and solid cross sections, respectively. This was likely attributed to the way that the fabric buckles. Due to its compliance, it may not have buckled or failed in the same position with each iterative experiment. The curve became more predictable with increasing pressures, and showed a higher resistance to bending at higher pressures. The higher pressure evaluated for the comparison of the two designs shown in Fig. 6d showed a deflection of $16.12 \pm 0.43^\circ$ for the solid cross section and $12.82 \pm 0.48^\circ$ for the hollow cross section for a 10 *N* load.

## IV. Experimental Validation of SR-AFO Exosuit

Stiffness characteristics of soft robots can be difficult to characterize on the user due to slippage or the compliance of the materials [19]. To address this challenge, a novel robotic approach was taken using two sets of validation experiments to determine the most accurate results of the performance of the SR-AFO exosuit. Quasi-static experimental protocols were implemented where the AFO is worn by the user during characterization to obtain stiffness values directly at the ankle joint. A total of six healthy participants were recruited for this study [age: 21 - 28 years, weight: 47.6 - 98.5 *kg*, height: 1.62 - 1.81 *m*], with three male and three female subjects. This study was approved by the Institutional Review Board of Arizona State University (STUDY00004351). For both protocols, the following seven conditions were evaluated for the SR-AFO exosuit: free foot (no SR-AFO exosuit), passive SR-AFO exosuit (0 *kPa*), and pressures of 10, 20, 30, 40, and 50 *kPa*. Pressure was capped at 50 *kPa* for the following trials for comfort reasons during prolonged static test environments. To minimize the effect of added stiffness due to muscle contraction, subjects were asked to relax their leg and ankle throughout the experimental trials. Muscle activity of 4 major ankle muscles was measured using surface electromyography (EMG) sensors: tibialis anterior (TA), medial gastrocnemius (GM), soleus (SL) and peroneus longus (PL). Before the experiment, muscle activity during fully relaxed and maximum voluntary contraction (MVC) was collected as per standard International Society of Electrophysiology and Kinesiology (ISEK) protocols [31].

### A. Methods

*1) SR-AFO Exosuit Stiffness in Sitting:* A quasi-static torque-angle relation was evaluated to determine the resulting

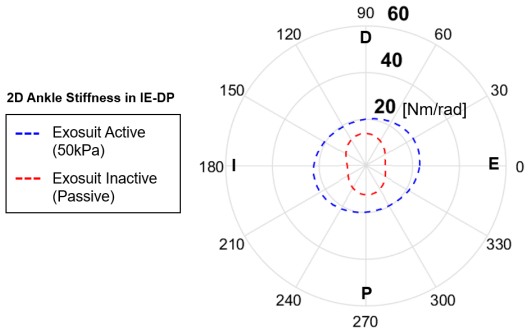


Fig. 8. Results from a representative subject showing ankle stiffness measured in 12 directions in a 2D polar plot, showing ankle stiffness with (50 *kPa*) and without (0 *kPa*) the SR-AFO exosuit active.

stiffness at the ankle joint with and without the SR-AFO exosuit active on the right foot of healthy participants ($n = 6$). A wearable robot, Anklebot (Interactive Motion Technologies, Inc.) was used to measure the 2D ankle stiffness in the sagittal and frontal planes [22], [32]. A specialized shoe connected the Anklebot on either side of the shoe behind the heel to interface the ankle with the Anklebot actuators. The Anklebot rotated the ankle in twelve directions in the 2D space, with axes that consisted of IE and DP directions (Fig. 7). This was repeated cyclically for three trials for each of the aforementioned conditions. A quasi-static test protocol was used to measure ankle stiffness in the 2D space, and the effective ankle stiffness for each of 12 movement directions was calculated from the continuous vector field and presented in a 2D polar plot (Fig. 8). Further details of this estimation method were described in previous work [32].

*2) SR-AFO Exosuit Stiffness in Quiet Standing:* Fig. 7b depicts the dual-axis robotic platform [23], [33] used to quantify the ankle stiffness in IE and DP of the right foot of healthy participants ($n = 6$). The robotic platform obtained kinematic data of the platform and the subjects ankle angle in IE and DP using a dual-axis goniometer (SG110, Biometrics Ltd, UK). The platform applied position perturbations to the ankle and measured the corresponding torques at the ankle using a force plate (9260AA3, Kistler, New York, USA) attached to the top of the platform, which was then used to estimate mechanical impedance of the ankle [34].

This study focused on the stiffness component of the ankle mechanical impedance, since ankle stiffness plays a major role in postural balance control during standing and locomotion tasks [34], [35]. The SR-AFO exosuit was evaluated for additional IE stiffness in the frontal plane for increasing pressure levels and monitored for maintaining relatively constant DP stiffness in the sagittal plane. Prior to the trial, subjects were asked to wear a pair of athletic shoes and their weight was recorded along with their natural center of pressure (CoP) of the right foot while standing upright on the platform. Wireless sEMG sensors were used to monitor the TA, GM, SL, and PL throughout the trials, and MVC of the muscle activity was collected prior to the trials. The subject was asked to stand with his/her right foot placed on the platform with the ankle axis of rotation aligned with that

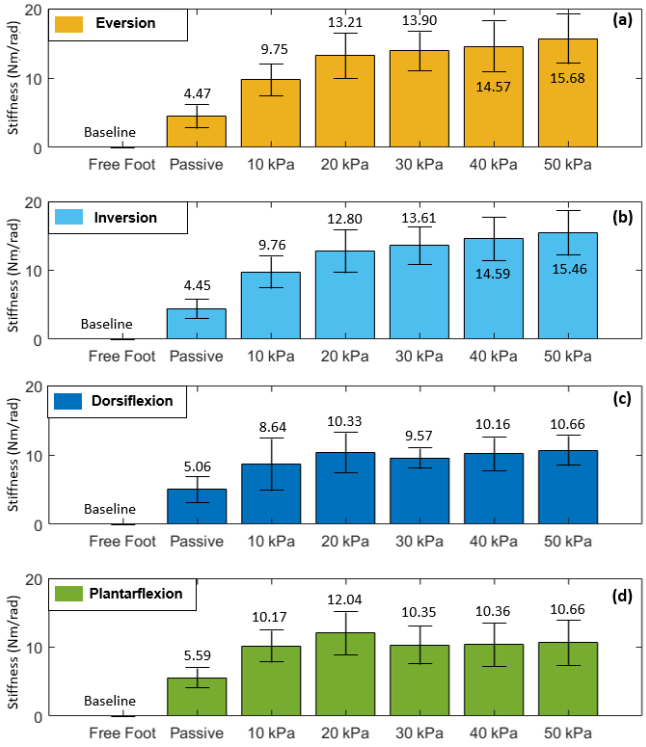


Fig. 9. Results of six healthy participants, characterizing ankle stiffness in the seven conditions shown, isolating the directions of the 2D polar plot to IE and DP axes to achieve ankle stiffness at the peak of each plane. The average value for each test condition is also displayed.

of the platform in the sagittal plane Fig. 7b. A vertical offset of the axis of rotation of the ankle vs. that of the platform in the frontal plane was accounted for as described in the aforementioned studies [34].

The platform applied a controlled rotational position perturbation in the direction of ankle eversion and dorsiflexion. A visual feedback system was provided to ensure that the subject had an equal weight distribution between each foot, and that the CoP of the right foot was maintained at the same point as measured during quiet standing before each perturbation was applied. A perturbation of 3° and a duration of 100 *ms* was applied in the eversion or dorsiflexion direction for a total of twelve trials.

## B. Results

*1) SR-AFO Exosuit Stiffness in Sitting:* Donning the SR-AFO exosuit inherently increased ankle stiffness in all directions. It was an anticipated result since the design of SR-AFO was based upon that of existing ankle wraps. This trend was consistent across all participants ($n = 6$). Group results for each of 4 directions in the frontal and sagittal planes are displayed in Fig. 9. After being asked to don the SR-AFO exosuit, subjects showed an average increase (i.e., increase from the baseline to the passive condition) of $4.45 \pm 1.42$ $Nm/rad$ of stiffness for inversion, $4.47 \pm 1.68$ $Nm/rad$ for eversion, $5.06 \pm 1.88$ $Nm$ for dorsiflexion, and $5.59 \pm 1.69$ $Nm/rad$ for plantarflexion. A trend of increasing ankle stiffness in the IE direction was observed over pressure levels up to 50 *kPa*, while there was an increase in stiffness

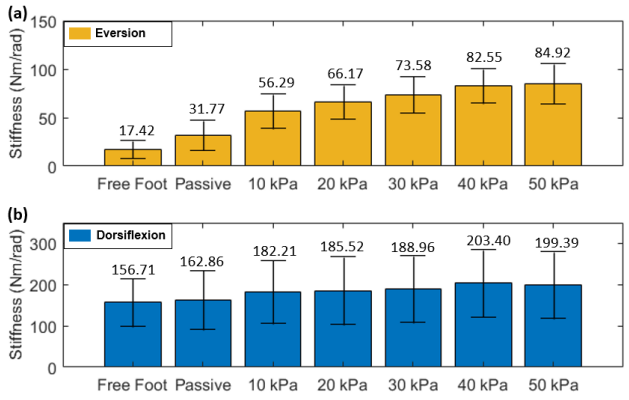


Fig. 10. Resulting ankle stiffness in (a) eversion and (b) dorsiflexion for each of the test conditions of the SR-AFO exosuit for a total of six healthy participants. The average value for each test condition is also displayed.

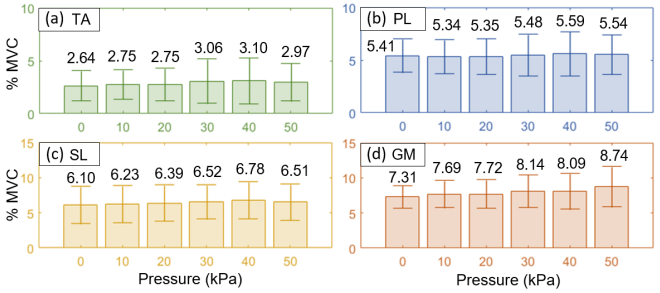


Fig. 11. Average muscle activation for each test condition with increasing pressure for the (a) TA, (b) PL, (c) SL, and (d) GM muscles while standing.

in the DP direction that plateaus at roughly 30 *kPa*. This was the point where the total volume of the actuator is filled and crumpling of the fabric against the human was no longer observed. A stiffness increase of 15.57± 3.41 $Nm/rad$ and 10.66 ± 2.72 $Nm/rad$ was observed at 50 *kPa* from the baseline for IE and DP directions, respectively. Although the degree of stiffness increase in the IE direction was about 50% greater than that the DP direction, it was significantly lower than the target IE stiffness (70 $Nm/rad$). Lower IE stiffness was likely due to slippage at the interface between the foot and SR-AFO exosuit under no loading in seated trials. This result emphasized the importance of characterizing the stiffness in standing conditions for which the exosuit was designed.

*2) SR-AFO Exosuit Stiffness in Quiet Standing:* Eversion stiffness showed a steady increasing trend to a maximum increase of 67.50 ± 16.75 $Nm/rad$ at 50 *kPa*, an increase by 387.5% from the original free foot stiffness (Fig. 10a) for eversion. In addition, it reached the target IE stiffness of 70 $Nm/rad$ at 30 *kPa*. The change of dorsiflexion stiffness was less noticeable than eversion stiffness. Dorsiflexion stiffness at 50 *kPa* increased by 22.4 % from the original free foot stiffness (Fig. 10b. The SR-AFO exosuit in its passive state was designed to resemble a basic ankle wrap, therefore a minor increase in stiffness was anticipated for passive trials. The stiffness measured in the standing position resulted in a much higher measured ankle stiffness in eversion than that of the seated trials. This can be attributed to the design of the anchoring points, which serves as a critical role in translating the forces of the soft actuators paired with the foot [19].

## V. Discussion

The SR-AFO exosuit was designed to be worn over the user‘s shoes and is simple to don/doff. The soft actuators were modeled with the assumption that a hollow beam design would be more effective than a solid beam of the same net volume in resisting deflection when a lateral load is applied. FEA and experimental results showed reduced deflection angle for the hollow beam design. The SR-AFO exosuit was tested with six healthy subjects using a wearable robot to measure and characterize ankle stiffness patterns. The Anklebot was used to measure 2D ankle stiffness in the IE and DP directions with the SR-AFO exosuit with the user sitting and the ankle left free to rotate across different pressure levels. The SR-AFO exosuit was also evaluated using a dual-axis robotic platform to measure 2D ankle stiffness during quiet standing. There is a major increase in stiffness between the sitting and standing trials, showing that the SR-AFO exosuit was not only effective under no loading, but was vastly more effective while the user was bearing weight on the ankle joint. The observed results during standing showed that the SR-AFO exosuit can effectively change eversion stiffness at the ankle joint from about 20 to 70 $Nm/rad$ at relatively low pressure levels (30 *kPa*), while minimizing the change in dorsiflexion stiffness in the sagittal plane. Ankle stiffness of 70 $Nm/rad$ in the frontal plane is significantly higher than the stiffness that unimpaired young individuals can achieve with the highest voluntary contraction of ankle muscles [22], [23]. Thus, the proposed design should be able to provide sufficient active support to the ankle in the frontal plane without constraining natural DP ankle movement in the sagittal plane.

The next stages of this research will focus on the controllability and portability of the system. While preliminary results and scope of this work showed a promise for static environments such as sitting and standing, the next iteration of this work will target dynamic tasks and include a custom pneumatic control board for the SR-AFO exosuit to investigate the effect of the AFO on kinematic and dynamic responses of the lower limb during various dynamic tasks including walking. This could be beneficial for looking at future applications where a soft AFO could be used as a standard for dynamic lateral ankle support during gait rehabilitation to replace the traditional rigid AFOs to help improve practice of physical therapists for rehabilitative exercises in both quiet standing and walking.

## Acknowledgements

C. M. Thalman is funded by the National Science Foundation GRFP award #1841051. This work is funded by the Global Sport Institute of the adidas and Arizona State University (ASU) Global Sport Alliance. The authors thank Varun Nalam, Tiffany Hertzell, and Kayleigh Gavin for their contribution.

## REFERENCES


[1] J. G. Garrick. The frequency of injury, mechanism of injury, and epidemiology of ankle sprains. *The American journal of sports medicine*, 5(6):241–242, 1977.

[2] K. Venesky, C. L Docherty, J. Dapena, and J. Schrader. Prophylactic ankle braces and knee varus-valgus and internal-external rotation torque. *Journal of athletic training*, 41(3):239, 2006.

[3] D. J. Caine, C. G. Caine, and K. J. Lindner. Epidemiology of sports injuries. *The Nurse Practitioner*, 21(9):142, 1996.

[4] J F Geboers, M R Drost, F Spaans, H Kuipers, and H A Seelen. Immediate and long-term effects of ankle-foot orthosis on muscle activity during walking: a randomized study of patients with unilateral foot drop. *Archives of physical medicine and rehabilitation*, 83(2):240–245, 2002.

[5] J. F Lehmann, S. M Condon, B. J de Lateur, and J C Smith. Ankle-foot orthoses: effect on gait abnormalities in tibial nerve paralysis. *Archives of physical medicine and rehabilitation*, 66(4):212–218, 1985.

[6] R B Stein, D G Everaert, A K Thompson, S Chong, M Whittaker, J Robertson, and G Kuether. Long-term therapeutic and orthotic effects of a foot drop stimulator on walking performance in progressive and nonprogressive neurological disorders. *Neurorehabilitation and neural repair*, 24(2):152–167, 2010.

[7] P. M Kluding, K. Dunning, M. W O'dell, S. S Wu, J. Ginosian, J. Feld, and K. McBride. Foot drop stimulation versus ankle foot orthosis after stroke: 30-week outcomes. *Stroke*, 44(6):1660–1669, 2013.

[8] J. S Jaivin, J. O Bishop, W G Braly, and H S Tullos. Management of acquired adult dropfoot. *Foot & ankle*, 13(2):98–104, 1992.

[9] P Malcolm, S Lee, S Crea, C Siviy, F Saucedo, I Galiana, F A Panizzolo, K G Holt, and C J Walsh. Varying negative work assistance at the ankle with a soft exosuit during loaded walking. *Journal of neuroengineering and rehabilitation*, 14(1):62, 2017.

[10] I. Wiszomirska, M. Błażkiewicz, K. Kaczmarczyk, G. Brzuszkiewicz-Kuźmicka, and A Wit. Effect of drop foot on spatiotemporal, kinematic, and kinetic parameters during gait. *Applied bionics and biomechanics*, 2017, 2017.

[11] J. Blaya and H. Herr. Adaptive control of a variable-impedance ankle-foot orthosis to assist drop-foot gait. *IEEE Transactions on neural systems and rehabilitation engineering*, 12(1):24–31, 2004.

[12] Jr MT Balmaseda, SH Koozekanani, MT Fatehi, C Gordon, PH Dreyfuss, and EC Tanbonliong. Ground reaction forces, center of pressure, and duration of stance with and without an ankle-foot orthosis. *Archives of physical medicine and rehabilitation*, 69(12):1009–1012, 1988.

[13] M. Yandell, B. Quinlivan, D. Popov, C. Walsh, and K. Zelik. Physical interface dynamics alter how robotic exosuits augment human movement: implications for optimizing wearable assistive devices. *Journal of neuroengineering and rehabilitation*, 14(1):40, 2017.

[14] S. Lee, S. Crea, P. Malcolm, I. Galiana, A. Asbeck, and C. Walsh. Controlling negative and positive power at the ankle with a soft exosuit. In *IEEE International Conference on Robotics and Automation (ICRA)*, pages 3509–3515. IEEE, 2016.

[15] C.M. Thalman, J. Hsu, L. Snyder, and P. Polygerinos. Design of a soft ankle-foot orthosis exosuit for foot drop assistance. In *2019 International Conference on Robotics and Automation (ICRA)*, pages 8436–8442. IEEE, 2019.

[16] J. Chung, R. Heimgartner, C. T. O'Neill, N. S. Phipps, and C. J. Walsh. Exoboot, a soft inflatable robotic boot to assist ankle during walking: Design, characterization and preliminary tests. In *2018 7th IEEE International Conference on Biomedical Robotics and Biomechatronics (Biorob)*, pages 509–516. IEEE, 2018.

[17] J. Kwon, J. Park, S. Ku, Y. Jeong, N. Paik, and Y.L. Park. A Soft Wearable Robotic Ankle-Foot-Orthosis for Post-Stroke Patients. *IEEE RA-L, International Conference on Soft Robotics (RoboSoft)*, 2019.

[18] C.M. Thalman, T Hertzell, and H Lee. Toward a soft robotic ankle-foot orthosis (sr-afo) exosuit for human locomotion: Preliminary results in late stance plantarflexion assistance. In *IEEE International Conference on Soft Robotics, (RoboSoft)*. IEEE, 2020. [Accepted].

[19] A.T. Asbeck, R.J. Dyer, A.F. Larusson, and C.J. Walsh. Biologically-inspired soft exosuit. In *2013 IEEE 13th International Conference on Rehabilitation Robotics (ICORR)*, pages 1–8, 2013.

[20] G. Bao, H. Fang, L. Chen, Y. Wan, F. Xu, Q. Yang, and L. Zhang. Soft robotics: Academic insights and perspectives through bibliometric analysis. *Soft Robotics*, 5(3):229–241, 2018.

[21] M. Cianchetti, C. Laschi, A. Menciassi, and P. Dario. Biomedical applications of soft robotics. *Nature Reviews Materials*, 3(6):143–153, 2018.

[22] H Lee, H Igo Krebs, and N Hogan. Multivariable dynamic ankle mechanical impedance with active muscles. *IEEE Transactions on Neural Systems and Rehabilitation Engineering*, 22(5):971–981, 2014.

[23] V. Nalam and H. Lee. Environment-dependent modulation of human ankle stiffness and its implication for the design of lower extremity robots. In *2018 15th International Conference on Ubiquitous Robots (UR)*, pages 112–118. IEEE, 2018.

[24] C Wielgosz et al. Bending and buckling of inflatable beams: some new theoretical results. *Thin-walled structures*, 43(8):1166–1187, 2005.

[25] Y. A. Seong, R. Niiyama, Y. Kawahara, and Y. Kuniyoshi. Low-pressure soft inflatable joint driven by inner tendon. In *2019 2nd IEEE International Conference on Soft Robotics (RoboSoft)*, pages 37–42. IEEE, 2019.

[26] F. Putzu, T. Abrar, and K. Althoefer. Plant-inspired soft pneumatic eversion robot. In *2018 7th IEEE International Conference on Biomedical Robotics and Biomechatronics (Biorob)*, pages 1327–1332. IEEE, 2018.

[27] J. Luong, P. Glick, A. Ong, M. S. deVries, S. Sandin, E. W. Hawkes, and M. T. Tolley. Eversion and retraction of a soft robot towards the exploration of coral reefs. In *2019 2nd IEEE International Conference on Soft Robotics (RoboSoft)*, pages 801–807. IEEE, 2019.

[28] C.M. Thalman, Q. P. Lam, P. H. Nguyen, S. Sridar, and P. Polygerinos. A novel soft elbow exosuit to supplement bicep lifting capacity. In *2018 IEEE/RSJ International Conference on Intelligent Robots and Systems (IROS)*, pages 6965–6971. IEEE, 2018.

[29] A. P. Boresi, R. J. Schmidt, O. M. Sidebottom, et al. *Advanced mechanics of materials*, volume 6. Wiley New York et al., 1985.

[30] EM Odom and CJ Egelhoff. Teaching deflection of stepped shafts: Castigliano's theorem, dummy loads, heaviside step functions and numerical integration. In *2011 Frontiers in Education Conference (FIE)*, pages F3H–1. IEEE, 2011.

[31] R. Merletti and P Di Torino. Standards for reporting emg data. *J Electromyogr Kinesiol*, 9(1):3–4, 1999.

[32] H. Lee, P. Ho, M. A Rastgaar, H. I Krebs, and N. Hogan. Multivariable static ankle mechanical impedance with relaxed muscles. *Journal of biomechanics*, 44(10):1901–1908, 2011.

[33] V. Nalam and H. Lee. Design and validation of a multi-axis robotic platform for the characterization of ankle neuromechanics. In *2017 IEEE International Conference on Robotics and Automation (ICRA)*, pages 511–516. IEEE, 2017.

[34] V Nalam and H Lee. Development of a two-axis robotic platform for the characterization of two-dimensional ankle mechanics. *IEEE/ASME Transactions on Mechatronics*, 24(2):459–470, 2019.

[35] D. A Winter. Human balance and posture control during standing and walking. *Gait & posture*, 3(4):193–214, 1995.